

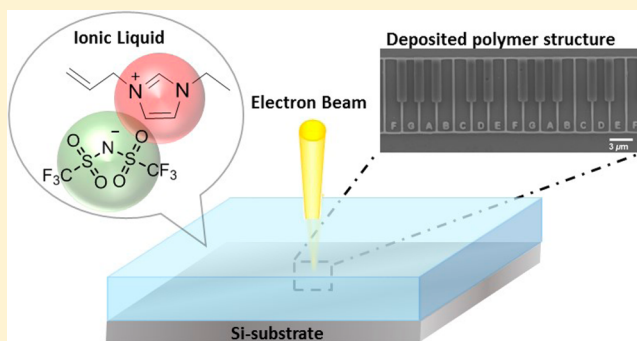
Polymerization of Room-Temperature Ionic Liquid Monomers by Electron Beam Irradiation with the Aim of Fabricating Three-Dimensional Micropolymer/Nanopolymer Structures

H. Minamimoto,[†] H. Irie,[†] T. Uematsu,^{†,‡} T. Tsuda,[†] A. Imanishi,[§] S. Seki,[†] and S. Kuwabata^{*,†}

[†]Department of Applied Chemistry, Graduate School of Engineering and [‡]Frontier Research Base for Global Young Researchers, Graduate of Engineering, Osaka University, 2-1 Yamada-oka, Suita, Osaka 565-0871, Japan

[§]Department of Chemistry, Graduate School of Engineering Science, Osaka University, 1-3 Machikaneyama, Toyonaka, Osaka 560-8531, Japan

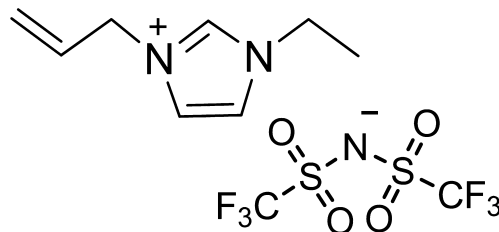
ABSTRACT: A novel method for fabricating microsized and nanosized polymer structures from a room-temperature ionic liquid (RTIL) on a Si substrate was developed by the patterned irradiation of an electron beam (EB). An extremely low vapor pressure of the RTIL, 1-allyl-3-ethylimidazolium bis((trifluoromethane)sulfonyl)amide, allows it to be introduced into the high-vacuum chamber of an electron beam apparatus to conduct a radiation-induced polymerization in the nanoregion. We prepared various three-dimensional (3D) micro/nanopolymer structures having high aspect ratios of up to 5 with a resolution of sub-100 nm. In addition, the effects of the irradiation dose and beam current on the physicochemical properties of the deposited polymers were investigated by recording the FT-IR spectra and Young's modulus. Interestingly, the overall shapes of the obtained structures were different from those prepared in our recent study using a focused ion beam (FIB) even if the samples were irradiated in a similar manner. This may be due to the different transmission between the two types of beams as discussed on the basis of the theoretical calculations of the quantum beam trajectories. Perceptions obtained in this study provide facile preparation procedures for the micro/nanostructures.



INTRODUCTION

Room-temperature ionic liquids (RTILs), which are liquid salts consisting only of cations and anions, have fascinated many researchers in various fields because of their unique physicochemical properties such as incombustibility, high ionic conductivity, high thermal stability, and wide electrochemical window.^{1–7} Among these properties, the negligible vapor pressure of RTILs is one of the most important features in recent research using RTILs under vacuum conditions.^{8,9} Our research group developed several new technologies that can be categorized as RTIL-vacuum technology.^{10,11} For example, we have developed an in situ scanning electron microscopy (SEM) technique to investigate electrochemical reactions in RTIL concurrently with the polarization of electrodes.^{12,13} In a series of investigations, we further noticed that certain types of chemical reactions, i.e., the reduction of metal ions, are induced by electron beam irradiation.^{14,15} The first finding was that gold particles were produced in an RTIL that contained gold ions during the observation of the RTIL by SEM. On the basis of these perceptions, we have established a completely new method to fabricate micro/nanosized polymer structures by drawing arbitrary patterns on a polymerizable RTIL, 1-allyl-3-ethylimidazolium bis((trifluoromethane)sulfonyl)amide ([AllylEtIm][Tf₂N], Scheme 1), with a focused

Scheme 1. Structure of Polymerizable RTIL, [AllylEtIm][Tf₂N]



ion beam (FIB) instrument.¹⁶ In this technique, we succeeded in fabricating various three-dimensional (3D) microscopic polymer structures that are difficult to build using conventional FIB techniques. The fabrication of complicated 3D structures was achieved by a distinctive formation mechanism that resembles the mechanism of 3D printers. The key point in this method is that the polymerization takes place at the RTIL/vacuum interface and that the reorganization of the liquid

Received: August 14, 2014

Revised: October 3, 2014

Published: October 16, 2014

meniscus raises the reaction position for the polymer structure to grow higher than the original thickness of the RTIL layer.

It is well known that ionizing radiation, e.g., γ -rays, X-rays, and electron beams, yields some kinds of reactive species in the area called “spur” where excitation and ionization occur.¹⁷ The reactive species indicated here are solvated electrons and radical ions. The mechanism for the formation of these species has widely been studied by many radiation chemists.^{18–20} These reactive species trigger several chemical reactions, such as the reduction of metal ions^{21,22} and cross-linking reactions.^{23,24} The reactive species generated by quantum beam irradiation on RTIL and chemical interactions between RTIL and ionizing radiation have attracted many researchers.^{25–29} According to previous studies, the radiolytic yield of solvated electrons in RTILs is higher than that in most organic solvents, and thus they could be very useful media for studies of radiolytic reactions such as electron transfer.²⁶ Additionally, many technologies combining RTILs and radiation techniques have been developed in recent years.^{30–32}

Recently, the demand for new methods of fabricating 3D micro/nanoscale structures has been increasing with respect to producing future microelectromechanical systems (MEMS), and there are many reports on new and innovative direct writing technologies.^{33–36} In this study, to extend our previous method¹⁶ and to propose our technique as a new direct writing method, we employed an electron beam (EB) writing system for the micro/nanofabrication of polymer structures from an allyl-type polymerizable RTIL. The EB has an advantage over the FIB in terms of higher resolution, although its energy density is lower. As a result, the structures obtained in the present study have higher resolution than those obtained in the FIB method. In addition, the results obtained in this study provide new insights for understanding the formation mechanism of the polymer structures, which is different between the FIB method and the present EB method. To the best of our knowledge, this is the first achievement that can control the polymerization of monomers on the sub-100-nm scale.

EXPERIMENTAL SECTION

Preparation of the RTIL-Coated Si Wafer and EB Irradiation Experiment. [AllylEtIm][Tf₂N] was purchased from Kanto Chemical Co., Inc. and used without further purification. An n-Si wafer (100 Ω cm⁻²) purchased from Osaka Titanium Technologies Co., Ltd. was used as a substrate. Water used in the present study was purified with a Milli-Q Integral 3 (18.2 M Ω cm). The sample preparation method was almost the same as the procedure described in our previous report.¹⁶ The Si substrate was cleaned in SC2 solution (conc. HCl/30% H₂O₂/H₂O = 1:1:4) at 60 °C for 20 min. Silicon atoms existing on the surface of the Si wafer were terminated with hydroxyl groups by UV/ozone treatment. To improve the affinity to the RTILs, the Si wafer was modified with 3-aminopropyltriethoxysilane (APTES). APTES aqueous solution (1 vol %) was placed on the substrate for 10 min,³⁷ followed by rinsing with ultrapure water. The appropriate amount of RTILs diluted with ethanol (5 vol %) was dropped onto the substrate and spun at 4000 rpm for 5 min. The thickness of the obtained liquid film was estimated by the reflectance measurement to be approximately 1 μ m.

The EB patterning was performed with a scanning electron microscope (JEOL-9100, JEOL Ltd.) equipped with a pattern generator (SPG-924, Sanyu Electron Co., Ltd.). EB irradiation was carried out in a vacuum chamber with its pressure kept under 9.6 \times 10⁻⁵ Pa. The acceleration voltage was 30 kV, and the beam current was adjusted from 1000 to 5000 pA. The shapes of drawing patterns were prepared in bitmap format (5000 pixels \times 5000 pixels) and fit into the

irradiation area of 50 μ m². Accordingly, the scale for 1 pixel becomes 10 nm². The EB was irradiated following the bitmap image in the raster scanning mode, and the scan rate was adjusted to give a designated electron dose. No recognizable changes in the pressure in the vacuum chamber were observed during irradiation. After EB exposure, the substrate was rinsed with acetonitrile to remove the unreacted RTIL and then dried in air. The prepared polymer patterns were observed by the SEM with an acceleration voltage of between 5 and 20 kV without a metal coating. An infrared spectrum was recorded with an FT-IR spectrometer (FT/IR-6200, JASCO), and that for the microstructure was measured with optional IR microscopy equipment (IRT-7200, Jasco). Raman spectra for both an ionic liquid and a deposited polymer were recorded with a Raman microscope (RAMAN-11, Nanophoton).

Measurement of Young's Modulus. The force curve measurements were performed with a scanning probe microscope (Nano-NaviReal, SII nanotechnology). A silicon cantilever (SI-DF20P) with a typical force constant of 9 N/m was employed. Prior to the force curve measurements, topographic images were recorded in tapping mode. Five arbitrary points were chosen for each polymer structure, and the repulsive forces were recorded as a function of the Z motion of sample stage. The force curves were fitted with the equation³⁸ by using an in-house procedure running on Igor Pro 6.3 (Wavemetrics Inc.) and the Young's modulus were estimated.

RESULTS

Fabrication of 3D Structures by EB Irradiation onto the Allyl-Type RTIL. The fabrication of 3D polymer structures from [AllylEtIm][Tf₂N], which was the same as the RTIL used in combination with FIB irradiation,¹⁶ was first demonstrated in the form of drawing some images and characters. Figure 1

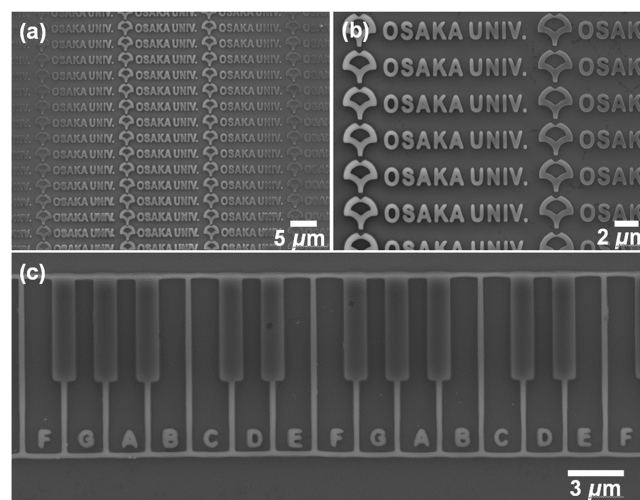


Figure 1. SEM images of polymer structures prepared by EB irradiation onto [AllylEtIm][Tf₂N]. (a) OSAKA UNIV. characters prepared over a 50 μ m² area, (b) magnified image of (a), and (c) keyboard layout. All of the structures were prepared under a 30 mC/cm² dose condition.

shows SEM images of the deposited polymers resulting from the irradiation of EB onto the [AllylEtIm][Tf₂N] layer that was spun onto the APTES-modified Si wafer. The fine structures were obtained according to the irradiation pattern with a uniform thickness of as large as 800 nm. Additionally, the magnified image also shows that this method achieves a resolution as small as around 200 nm. As judged from the rigid nature of the structures that were retained on the substrate even after multiple rinsing, some chemical bonds may be formed between the polymer and surface modifier during irradiation

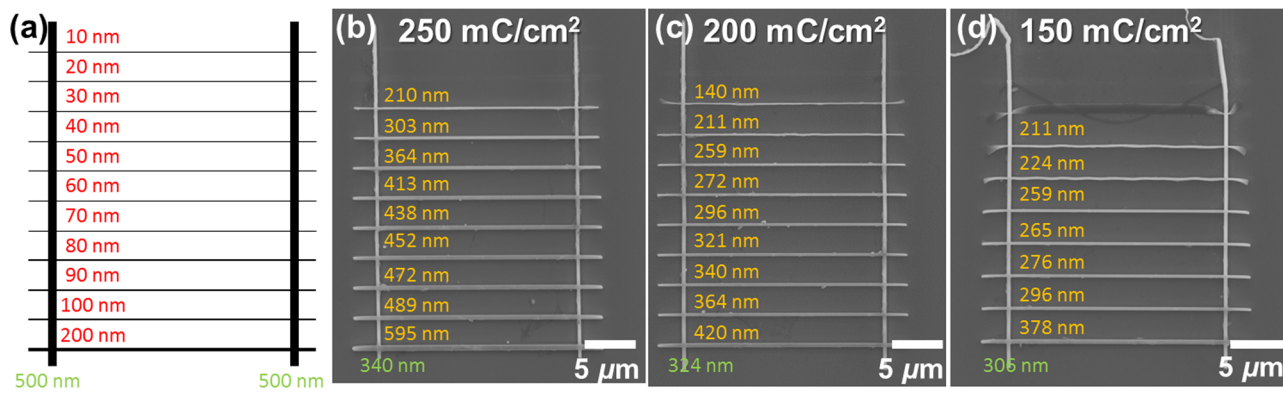


Figure 2. Line patterns prepared to check the resolution. (a) Irradiation design with the numbers indicating the width of each line: red for horizontal lines and green for vertical lines. (b–d) SEM images of deposited structures prepared under dose conditions of (b) 250, (c) 200, and (d) 150 mC/cm². The numbers in orange and green indicate the actual line widths of the obtained structures for horizontal and vertical lines, respectively.

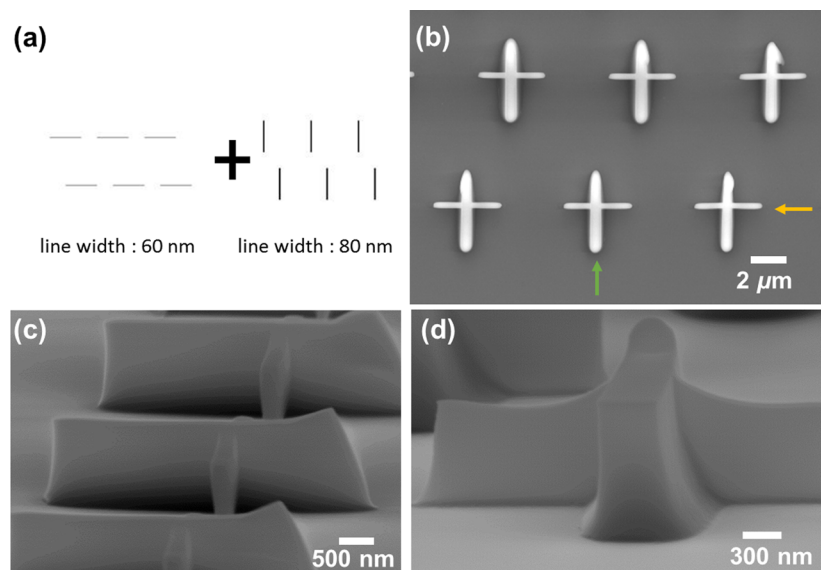


Figure 3. Cross-shaped structures prepared by two-step irradiation: (a) irradiation design indicating the two-step irradiation, (b) top-view SEM image of deposited structures, (c, d) side-view SEM images observed from the direction represented in (b) by (c) orange and (d) green arrows. The dose condition was 200 mC/cm².

more than for a simple physisorption. The irradiated dose per unit area was 30 mC/cm² (900 J/cm²), which is much higher than that used for EB lithography with a commercially available resist of ca. 10 μC/cm² (300 mJ/cm²) in the case of negative type SU-8.³⁹ Besides the intrinsic reason that the polymerization of monomers needs a higher electron dose than cross-linking reactions, the need for such large doses is due to the low reactivity of the allyl group leading to cross-linking chain transfer, as is well known. Incidentally, we could not obtain any structures when the irradiation dose was less than 20 mC/cm²; there was a definite threshold for obtaining a solid deposition probably because of the requirement of generating the insoluble oligomers and low-molecular-weight polymers.

Polymer line structures as illustrated in Figure 2 were fabricated to demonstrate the resolution of the resulting polymer pattern. Eleven lines with different widths were aligned parallel to each other with two thick vertical lines that were formed prior to the formation of the horizontal lines in order to maintain the uniformity of the RTIL thickness of this area. SEM images for the thus-formed polymer structures are shown in Figure 2b–d with the dose per unit area given to make each

structure. The first thing we should mention is that not all of the lines were formed as irradiated. In the cases of 250 and 200 mC/cm², the two narrowest horizontal lines (10 and 20 nm) were not obtained, and when the dose was reduced to 150 mC/cm², the line of 30 nm width was also absent. As we mentioned in the Experimental Section, the line of 10 nm width corresponds to that of 1 pixel width; in other words, the electron beam is scanned one time in raster scanning mode used in a series of experiments. These results indicate that not only the dose per unit area but also the consecutive irradiation of EB to adjacent positions has some influence on the formation of solid structures, which is quite unexpected if the nature of liquids and the typical scan interval (about 0.3 s) are considered. It is also noteworthy that the difference in width between the irradiation pattern and the obtained polymer pattern for the horizontal lines became large with an increase in dose whereas that for vertical lines became small.

SEM images in Figure 3 show cross-shaped patterns composed of horizontal and vertical lines. The irradiation design of each line has 60 and 80 nm width, respectively. It must be noted that the horizontal lines were first drawn,

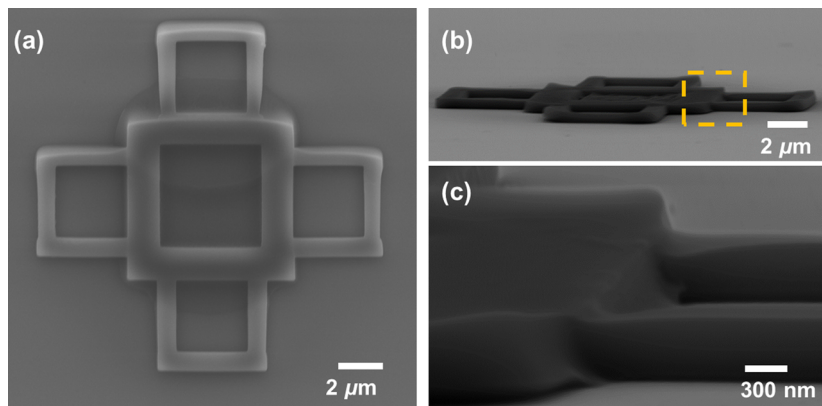


Figure 4. SEM image of frame structure composed of five squares: (a) top view, (b) side view, and (c) magnified image of the orange square in (b). The dose condition was $30 \text{ mC}/\text{cm}^2$.

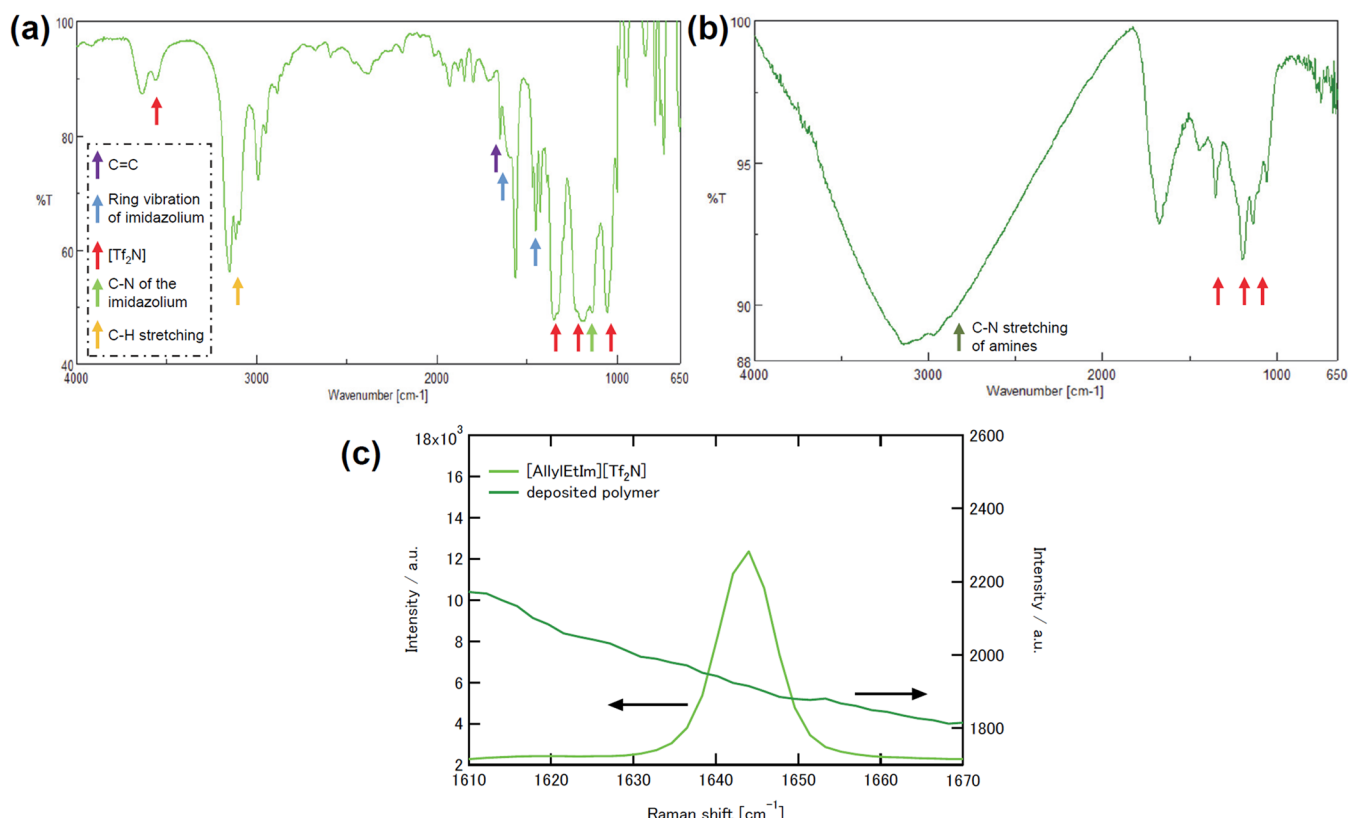


Figure 5. (a) FT-IR spectrum of $[\text{AllylEtIm}][\text{Tf}_2\text{N}]$, (b) FT-IR microscopic measurement for the deposited polymer structures, and (c) micro Raman spectra of deposited polymer structures (ex. 532 nm). The light and dark green lines indicate the RTIL monomer and deposited polymer, respectively.

followed by drawing the vertical lines; the irradiation dose for both lines was $200 \text{ mC}/\text{cm}^2$, which is large enough to obtain polymers from the perspective given above. SEM images from different angles are also shown in Figure 3c,d. Even both structures were fabricated under the same condition; there was a distinct difference in height between them. The dose may not be an exclusive factor that decides the thickness of the structure.

To investigate the effect of two-step irradiation on the deposited shape and to compare the present method to the previous FIB method, we irradiated EB by following the irradiation design that we have used in the previous FIB experiment. The structures in Figure 4 were composed of five square frames; a bigger center frame was first prepared,

followed by four smaller frames with one side of each frame being overlapped with the center frame. Unlike the jack-in-a-box-like structures prepared by FIB irradiation with raster scanning (Figure 5C in ref 16), all of the frames were attached on the Si substrate independently of the order of irradiation, as if they have grown from the substrate. It is one of the most important differences seen between FIB and EB irradiation.

Characterization of the Deposited Polymer Structures by FT-IR Spectroscopy. To understand the chemical reactions, the structures in Figure 1 were characterized by FT-IR microscopic analysis. The beam size of the IR microscope was confined to $10 \mu\text{m}^2$ by an aperture, and a part of the structure was measured. The IR spectra for both the

Table 1. Results of Young's Modulus Measurements for Each Polymer Structure

measuring points	polymer structures deposited by a beam current of 1 nA		polymer structures deposited by a beam current of 2.5 nA		polymer structures deposited by beam current of 5 nA	
	E (Gpa) for 50 mC/cm ²	E (Gpa) for 100 mC/cm ²	E (Gpa) for 50 mC/cm ²	E (Gpa) for 100 mC/cm ²	E (Gpa) for 50 mC/cm ²	E (Gpa) for 100 mC/cm ²
1	6.0	80	0.2	12	2.3	70
2	1.4	40	50	180	0.3	100
3	0.5	80	25	50	15	3.5
4	<0.1 ^a	1.0	<0.1 ^a	150	30	100
5	<0.1 ^a	40	180	30	40	60

^aFitting reliability is low for soft samples, less than 0.1 GPa.

[AllylEtIm][Tf₂N] monomer and deposited structures are shown in Figure 5a,b. In the spectrum of the monomer, the multiple peaks around 3100 cm⁻¹ are derived from C—H stretching of the imidazolium cation. The absorption band around 1136 cm⁻¹ was assigned to the C—N symmetric and asymmetric stretching of the imidazolium side chain, and the sharp peak at 1624 cm⁻¹ and multiple peaks around 1452 cm⁻¹ are derived from the ring vibration of imidazolium. The C=C stretching for the allyl group arises as a small peak at 1649 cm⁻¹. On the contrary, vibrations for [Tf₂N] anion are observed at 3636, 3552, 1356, 1190, and 1056 cm⁻¹. After the EB irradiation to [AllylEtIm][Tf₂N], the IR spectrum changed drastically. The most distinctive difference is the broad absorption between 2500 and 3500 cm⁻¹ that is attributable to the N—H stretching of amines (including some coupled overtone vibrations) in a complicated chemical environment.⁴⁰ The small peak arising from the allyl group disappeared, whereas absorptions corresponding to [Tf₂N] were almost unchanged. The disappearance of the allyl group was also confirmed by the micro Raman spectra that were more sensitive to the C=C double bond (Figure 5c). These results indicate that the majority of the radiation-induced reaction occurs on the cation, leading to the cleavage of C—N bonds for side chains⁴¹ and to the oligomerization of allyl group. A cross-linking reaction may also occur to form deposits during the continuous irradiation of EB at a relatively high dose.

Measurement of Young's Modulus by AFM. The elastic properties of the deposited polymer were examined by AFM in the force curve mode, which measures the repulsive force from the sample indented by a cantilever. The displacement of the cantilever, $z - z_0$, and the sample distortion, $d - d_0$, can be associated with the following equation³⁸

$$z - z_0 = d - d_0 + \sqrt{\frac{k(d - d_0)}{\left(\frac{2}{\pi}\right)[E(1 - \nu^2)]\tan(\alpha)}} \quad (1)$$

where k is the spring constant of the cantilever, E is the Young's modulus of the sample, α is the half-opening angle of the cone ($= 16^\circ$), and ν is a Poisson ratio that is equal to 0.5. The cantilever's spring constant k was estimated by eq 1 on the basis of the force curve on a Si substrate having a known elasticity of $E = 185$ GPa. Then, the Young's modulus of the samples were estimated by fitting the force curves to the equation. More detailed information about this method has been reported by Radmacher.³⁸

The elasticity of the structures made with six different irradiation conditions are listed in Table 1; five points were chosen at random for each structure. No discernible difference could be identified from SEM observations between these points of measurement. At first glance, the deposited polymers

had nonuniform structures with different Young's moduli by location. However, the elasticity of each polymer was still correlated with the dose amount and beam current when they are compared as an average. Commercially available polymers, such as polyethylene and poly(ethylene terephthalate), have a Young's modulus of around 10 GPa.⁴² Under all current conditions between 1 and 5 nA, the doses seemed to have a major effect on the elasticity of the samples. The structures prepared with 100 mC/cm² were much harder than those deposited with 50 mC/cm². We can easily expect that the chemical structures of the polymer may be changed by long-time EB irradiation. It is also notable that the number of relatively hard points, for example, $E > 50$ GPa for 50 mC/cm² and $E > 100$ GPa for 100 mC/cm², became large with the increase in the beam current, suggesting that not only the dose but also the beam current has an effect on the physical properties of the polymer.

DISCUSSION

It is commonly known that the allyl groups are hardly polymerized because generated radicals are too stable to obtain successive radical polymerization reactions.⁴³ However, we obtained solid structures by FIB irradiation to the allyl-functionalized RTIL, which was reported recently with a possible mechanism of the chemical reactions.¹⁶ [AllylEtIm][Tf₂N] oligomers were considered to be first formed by repeated ion beam irradiation, followed by the cross-linking reaction between these oligomers. Thus, the rigid polymer structures have been obtained from the allyl-functionalized ionic liquid. The same reactions may also be induced by the irradiation of EB. The results of FT-IR and Young's modulus measurements, which revealed that larger doses lead to the formation of stiff structures with complicated chemical structure, show the occurrence of the cross-linking reaction and support our prognosis.

One of the important points for our present technique is that we can make any shape of deposits precisely by a single raster writing of images. Even if the irradiation area exceeds 50 × 50 μm, the obtained structure had a resolution of several tens of nanometers. The resolution of polymers produced by EB irradiation was further examined by using the image shown in Figure 2a. The most notable thing is the absence of some lines. In the case of 250 and 200 mC/cm², for example, at least three scans were required to obtain the polymer structure, indicating the cumulative effect of three adjacent temporally spaced shots. This in itself is not strange if it was considered that the spatial spread of the electron range around several tens of nanometers in radius, as will be mentioned later, increases the net dose of the overlapped place. In such a case, however, the active species must stay in the same position and alive during a scanning

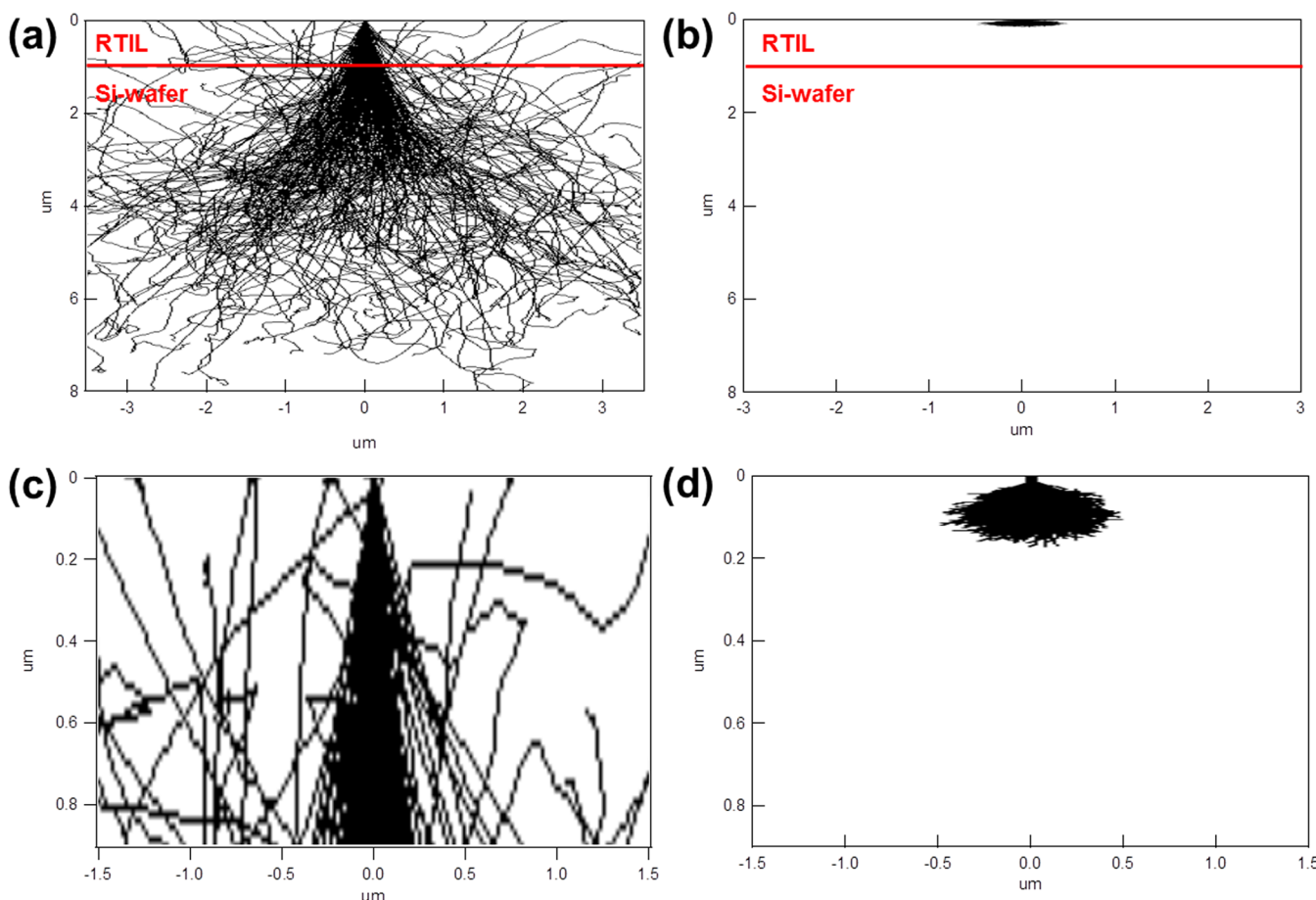


Figure 6. Monte Carlo simulation for (a) the electron range and (b) the ion range. The images in (c) and (d) are the magnified graphs for the RTIL layer of (a) and (b), respectively. The number of incident electrons and ions was 10 000. The displayed electron number is 200. The thickness of an RTIL layer was 1 μm , and the density of [allylEtIm][Tf₂N] was 1.46 g cm^{-3} . The black lines were the trajectory of incident particles. These simulation were performed by CASINO for the electron range and SRIM 2008 for the ion range.

interval of typically 0.3 s. Calculation from the diffusion coefficient of RTILs, which is on the order of $1 \times 10^{-11} \text{ m}^2 \text{ s}^{-1}$, predicts that the reactive species generated in spurs can travel ca. 1 μm from the irradiated positions during that interval time.⁴⁴ In addition, the lifetime of the reactive species is several tens of microseconds is too short to maintain its chemical reactivity over repetitive scans.²⁸ Therefore, it is most plausible that the oligomers having a much lower diffusivity than monomers that are formed during the first and second scan, and then they are deposited to form the rigid structure by the third scan.

Differences that cannot be ignored between the irradiation line width and the actual width of the corresponding deposits should be considered. It is quite reasonable to consider the traveling of electrons after they hit the material. The electron range, which indicates the distance from the surface of the target to the position where irradiated electrons completely lose their energy, can be calculated from the following equation

$$R = 2.1 \times 10^{-12} \times \frac{E_0^2}{\rho} \quad (2)$$

where E_0 (eV) is the energy of irradiated electrons and ρ (g/cm^{-3}) is the density of the target. In the case of [AllylEtIm][Tf₂N] with a density of $\rho = 1.46 \text{ g}/\text{cm}^{-3}$,¹⁶ the electron range is estimated to be approximately 13 μm , which is much larger than the RTIL layer thickness that is as small as 1 μm . Of

course, a lateral displacement should also occur via electron scattering during the travel within the RTIL layer. The Monte Carlo simulation was therefore employed to draw trajectories of multiple sets of electrons by assuming a two-layer model consisting of 1 μm RTIL and a Si wafer (density 2.3 g/cm^{-3}) as a bottom layer.⁴⁵ As shown in Figure 6a, a large part of the electrons penetrate the RTIL layer and reach the Si substrate, with the expansion of beam diameter in RTILs due to the elastic and inelastic scattering. The lateral spreading of electrons reaches up to several tens of nanometers, and it becomes obvious at high doses. These perceptions coincided with the results shown in Figure 2, where a high dose gave thick structures even if the same irradiation pattern was used. In other words, a high-resolution structure can be obtained by the appropriate choice of the dose. In fact, the structures made for demonstration (Figure 1) were prepared at a much lower dose (30 mC/cm^2) than that displayed in Figures 2 and 3 composed of narrower lines. Together with the perceptions mentioned above, preparation of the bulky structure needs less dose because the oligomers have many chances to be solidified by the EB irradiated in close proximity.

The polymer structures shown in Figure 3 provide another interesting point of view. The tilt SEM images show that the line structures have a high aspect ratio up to around 5. Such a high aspect ratio can be obtained only by recently developed new resist materials such as an epoxy chemistry-based EB resist

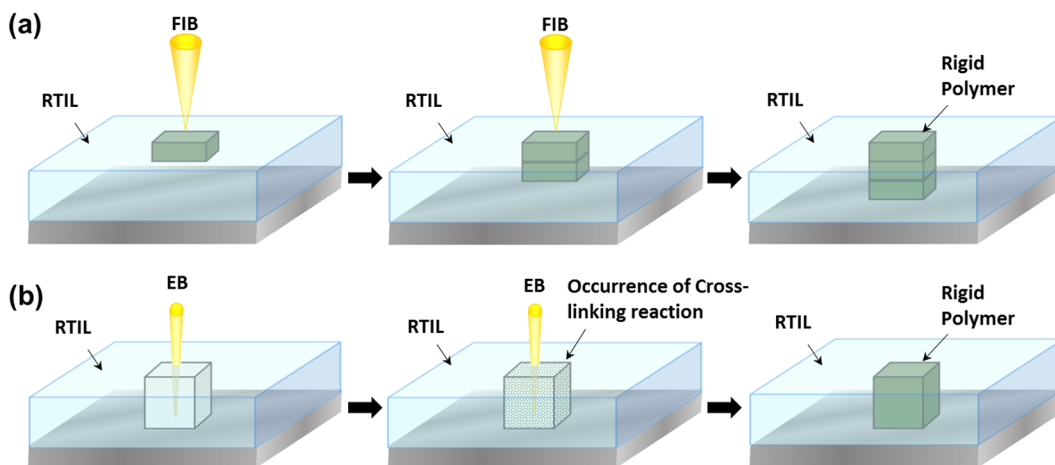


Figure 7. Illustrations of the polymer formation mechanism for (a) the FIB-RTIL method and (b) the EB-RTIL method. In the case of the FIB method, the polymer structures were deposited on the surface of the RTIL. On the contrary, the polymer patterns were formed between the substrate and RTIL by EB irradiation.

and chemically amplified resists.^{35,46–48} The ease of the rinsing process that is intrinsic to the liquid matrix may contribute to the achievement because in the conventional lithographic processes mechanical stress between the developed structures and nonreacted polymer matrix often damage the spindly part of structures during the rinsing process.⁴⁹ This stressless situation seemed to bring another advantage that is the smoothness of the sidewalls, the roughness of which was hardly recognized in the SEM images shown in Figure 3. The difference in height between the horizontal and vertical lines should also be discussed. Although the dose was the same in both cases, the vertical lines were higher than the horizontal ones. This may derive from the alteration of the RTIL thickness that was pushed up by the predeposited horizontal structures, making the second vertical structures grow higher than the horizontal ones. Such a phenomenon seems to be unique to the liquid-phase reaction and could not be observed for the case of the common resist materials. Furthermore, the horizontal structures were gently curving around the intersection with the vertical lines, as shown in Figure 3d, probably because the growth around the curved area was initiated from the top of the existing horizontal line during the preparation of the vertical lines. This can be predicted from the result of the Monte Carlo simulation. These behaviors are very different from not only the conventional lithography but also from our previous FIB-RTIL method in which the two-step exposure can realize complicated 3D structures including both hollow and reverse taper structures.¹⁶

The structure shown in Figure 4 is a typical example that expresses the differences between the EB and FIB methods. Although in the FIB method the four smaller squares were deposited on the center square so as to be completely lifted from the Si substrate (Figure 5C in ref 16), all five frames were deposited on the substrate when the EB was used. To understand these different phenomena, the Monte Carlo simulation was also performed for the diffusion of the Ga ion beam at 30 kV in the RTIL layer and was displayed in Figure 6b.⁵⁰ In the case of ion beam irradiation at an accelerating voltage of 30 kV, the Ga ion range was considerably smaller than the electron range because of its strong interaction with atoms in the target RTIL. Therefore, as shown in Figure 7, we can conclude that the polymers prepared by the FIB irradiation form at the interface of vacuum and RTIL, whereas in the case

of the EB irradiation a large part of the electrons penetrate the RTIL layer and the polymerization and cross-linking reaction occur over the whole irradiated area of the RTIL at once. By considering all results, which we obtained in the present study, we were able to clarify the difference between EB-RTIL and FIB-RTIL methods, and we also found the utility of each quantum beam RTIL method.

CONCLUSIONS

We fabricated fine polymer structures with a high aspect ratio and high resolution over an area as large as $50 \times 50 \mu\text{m}$ by introducing the allyl-type polymerizable RTIL into the EB drawing system. The formation mechanism of the polymer structures was discussed and compared with the recent report that used the FIB. From all results given in this article, we propose the idea of a completely new direct writing technique, and we strongly believe that this development will become a viable technology for the fabrication of micromachines or microelectronic devices.

AUTHOR INFORMATION

Corresponding Author

*E-mail: kuwabata@chem.eng.osaka-u.ac.jp.

Author Contributions

S.K., T.T., A.I., and S.S. designed the experiment. H.M. and H.I. prepared the samples and performed experiments. H.M., H.I., and T.U. analyzed and interpreted the results. H.M., T.U., and S.K. developed the model. H.M., T.U., and S.K. prepared the manuscript.

Notes

The authors declare no competing financial interest.

ACKNOWLEDGMENTS

We express our appreciation to Prof. M. Ozaki and Prof. H. Yoshida of the Division of Electrical Electronic and Information Engineering, Osaka University, for performing the reflectance measurement to estimate the thickness of the RTIL layers. This study was supported by the Core Research for Evolution Science and Technology (CREST) from the Japan Science and Technology Agency (JST).

■ REFERENCES

- (1) Bonhôte, P.; Dias, A.-P.; Papageorgiou, N.; Kalyanasundaram, K.; Grätzel, M. Hydrophobic, Highly Conductive Ambient-Temperature Molten Salts. *Inorg. Chem.* **1996**, *35*, 1168–1178.
- (2) Huddleston, J. G.; Visser, A. E.; Reichert, W. M.; Willauer, H. D.; Broker, G. A.; Rogers, R. D. Characterization and Comparison of Hydrophilic and Hydrophobic Room Temperature Ionic Liquids Incorporating the Imidazolium Cation. *Green Chem.* **2001**, *3*, 156–164.
- (3) Rogers, R. D.; Seddon, K. R. Chemistry. Ionic Liquids—Solvents of the Future? *Science* **2003**, *302*, 792–793.
- (4) Zhou, Z.-B.; Matsumoto, H.; Tatsumi, K. Low-Melting, Low-Viscous, Hydrophobic Ionic Liquids: *N*-Alkyl(alkyl Ether)-*N*-Methyl-pyrrolidinium Perfluoroethyltrifluoroborate. *Chem. Lett.* **2004**, *33*, 1636–1637.
- (5) Earle, M. J.; Esperança, J. M. S. S.; Gilea, M. A.; Canongia Lopes, J. N.; Rebelo, L. P. N.; Magee, J. W.; Seddon, K. R.; Widegren, J. A. The Distillation and Volatility of Ionic Liquids. *Nature* **2006**, *439*, 831–834.
- (6) Hapiot, P.; Lagrost, C. Electrochemical Reactivity in Room-Temperature Ionic Liquids. *Chem. Rev.* **2008**, *108*, 2238–2264.
- (7) Armand, M.; Endres, F.; MacFarlane, D. R.; Ohno, H.; Scrosati, B. Ionic-Liquid Materials for the Electrochemical Challenges of the Future. *Nat. Mater.* **2009**, *8*, 621–629.
- (8) Lovelock, K. R. J.; Villar-Garcia, I. J.; Maier, F.; Steinrück, H.-P.; Licence, P. Photoelectron Spectroscopy of Ionic Liquid-Based Interfaces. *Chem. Rev.* **2010**, *110*, 5158–5190.
- (9) Huang, J. Y.; Zhong, L.; Wang, C. M.; Sullivan, J. P.; Xu, W.; Zhang, L. Q.; Mao, S. X.; Hudak, N. S.; Liu, X. H.; Subramanian, A.; et al. In Situ Observation of the Electrochemical Lithiation of a Single SnO₂ Nanowire Electrode. *Science* **2010**, *330*, 1515–1520.
- (10) Kuwabata, S.; Tsuda, T.; Torimoto, T. Room-Temperature Ionic Liquid. A New Medium for Material Production and Analyses under Vacuum Conditions. *J. Phys. Chem. Lett.* **2010**, *1*, 3177–3188.
- (11) Torimoto, T.; Tsuda, T.; Okazaki, K.; Kuwabata, S. New Frontiers in Materials Science Opened by Ionic Liquids. *Adv. Mater.* **2010**, *0871*, 1196–1221.
- (12) Arimoto, S.; Oyamatsu, D.; Torimoto, T.; Kuwabata, S. Development of in Situ Electrochemical Scanning Electron Microscopy with Ionic Liquids as Electrolytes. *ChemPhysChem* **2008**, *9*, 763–767.
- (13) Uematsu, T.; Han, J.-T.; Tsuda, T.; Kuwabata, S. Metal-Ion Diffusion in Ionic Liquid Studied by Electrochemical Scanning Electron Microscopy with X-Ray Fluorescence Spectrometry. *J. Phys. Chem. C* **2012**, *116*, 20902–20907.
- (14) Imanishi, A.; Tamura, M.; Kuwabata, S. Formation of Au Nanoparticles in an Ionic Liquid by Electron Beam Irradiation. *Chem. Commun.* **2009**, 1775–1777.
- (15) Imanishi, A.; Gonsui, S.; Tsuda, T.; Kuwabata, S.; Fukui, K. Size and Shape of Au Nanoparticles Formed in Ionic Liquids by Electron Beam Irradiation. *Phys. Chem. Chem. Phys.* **2011**, *13*, 14823–14830.
- (16) Kuwabata, S.; Minamimoto, H.; Inoue, K.; Imanishi, A.; Hosoya, K.; Uyama, H.; Torimoto, T.; Tsuda, T.; Seki, S. Three-Dimensional Micro/nano-Scale Structure Fabricated by Combination of Non-Volatile Polymerizable RTIL and FIB Irradiation. *Sci. Rep.* **2014**, *4*, 3722.
- (17) Shkrob, I. A.; Marin, T. W.; Chemerisov, S. D.; Hatcher, J.; Wishart, J. F. Toward Radiation-Resistant Ionic Liquids. Radiation Stability of Sulfonyl Imide Anions. *J. Phys. Chem. B* **2012**, *116*, 9043–9055.
- (18) Shkrob, I. A.; Marin, T. W.; Chemerisov, S. D.; Wishart, J. F. Radiation Induced Redox Reactions and Fragmentation of Constituent Ions in Ionic Liquids. 1. Anions. *J. Phys. Chem. B* **2011**, *115*, 3872–3888.
- (19) Shkrob, I. A.; Marin, T. W.; Chemerisov, S. D.; Hatcher, J. L.; Wishart, J. F. Radiation Induced Redox Reactions and Fragmentation of Constituent Ions in Ionic Liquids. 2. Imidazolium Cations. *J. Phys. Chem. B* **2011**, *115*, 3889–3902.
- (20) Marcinek, A.; Zielonka, J.; Gębicki, J.; Gordon, C. M.; Dunkin, I. R. Ionic Liquids: Novel Media for Characterization of Radical Ions. *J. Phys. Chem. A* **2001**, *105*, 9305–9309.
- (21) Dey, G. R.; El Omar, A. K.; Jacob, J. A.; Mostafavi, M.; Belloni, J. Mechanism of Trivalent Gold Reduction and Reactivity of Transient Divalent and Monovalent Gold Ions Studied by Gamma and Pulse Radiolysis. *J. Phys. Chem. A* **2011**, *115*, 383–391.
- (22) Ma, J.; Zou, Y.; Jiang, Z.; Huang, W.; Li, J.; Wu, G.; Huang, Y.; Xu, H. An in Situ XAFS Study—the Formation Mechanism of Gold Nanoparticles from X-ray-Irradiated Ionic Liquid. *Phys. Chem. Chem. Phys.* **2013**, *15*, 11904–11908.
- (23) April, R. Crosslinking of Polymers in Solution. *J. Phys. Chem.* **1958**, *63*, 1852–1858.
- (24) Maeyoshi, Y.; Takano, K.; Asano, A.; Marui, H.; Omichi, M.; Satoh, T.; Kamiya, T.; Ishii, Y.; Ohkubo, T.; Koka, M.; et al. Fabrication of Poly(9,9'-Diocetylfluorene)-Based Nano- and Microstructures by Proton Beam Writing. *Jpn. J. Appl. Phys.* **2012**, *51*, 045201.
- (25) Behar, D.; Gonzalez, C.; Neta, P. Reaction Kinetics in Ionic Liquids: Pulse Radiolysis Studies of 1-Butyl-3-Methylimidazolium Salts. *J. Phys. Chem. A* **2001**, *105*, 7607–7614.
- (26) Wishart, J. F.; Neta, P. Spectrum and Reactivity of the Solvated Electron in the Ionic Liquid Methyltributylammonium Bis(trifluoromethylsulfonyl)imide. *J. Phys. Chem. B* **2003**, *107*, 7261–7267.
- (27) Takahashi, K.; Sato, T.; Katsumura, Y.; Yang, J.; Kondoh, T.; Yoshida, Y.; Katoh, R. Reactions of Solvated Electrons with Imidazolium Cations in Ionic Liquids. *Radiat. Phys. Chem.* **2008**, *77*, 1239–1243.
- (28) Fu, H.; Xing, Z.; Cao, X.; Wu, G. Pulse Radiolysis Studies of Functionally Substituted Imidazolium-Based Ionic Liquids. *Chin. Sci. Bull.* **2012**, *57*, 2752–2758.
- (29) Wishart, J. F. Ionic Liquids and Ionizing Radiation: Reactivity of Highly Energetic Species. *J. Phys. Chem. Lett.* **2010**, *1*, 3225–3231.
- (30) Tsuda, T.; Sakamoto, T.; Nishimura, Y.; Seino, S.; Imanishi, A.; Kuwabata, S. Various Metal Nanoparticles Produced by Accelerated Electron Beam Irradiation of Room-Temperature Ionic Liquid. *Chem. Commun.* **2012**, *48*, 1925–1927.
- (31) Roy, P.; Lynch, R.; Schmuki, P. Electron Beam Induced in-Vacuo Ag Deposition on TiO₂ from Ionic Liquids. *Electrochim. Commun.* **2009**, *11*, 1567–1570.
- (32) Radha, B.; Kiruthika, S.; Kulkarni, G. U. Metal Anion-Alkyl Ammonium Complexes as Direct Write Precursors to Produce Nanopatterns of Metals, Nitrides, Oxides, Sulfides, and Alloys. *J. Am. Chem. Soc.* **2011**, *133*, 12706–12713.
- (33) Bhuvana, T.; Kulkarni, G. U. Highly Conducting Patterned Pd Nanowires by Direct-Write Electron Beam Lithography. *ACS Nano* **2008**, *2*, 457–462.
- (34) Radha, B.; Kiruthika, S.; Kulkarni, G. U. Metal Anion-Alkyl Ammonium Complexes as Direct Write Precursors to Produce Nanopatterns of Metals, Nitrides, Oxides, Sulfides, and Alloys. *J. Am. Chem. Soc.* **2011**, *133*, 12706–12713.
- (35) Igaki, J.; Kanda, K.; Haruyama, Y.; Ishida, M.; Ochiai, Y.; Fujita, J.; Kaito, T.; Matsui, S. Comparison of FIB-CVD and EB-CVD Growth Characteristics. *Microelectron. Eng.* **2006**, *83*, 1225–1228.
- (36) Gerasimov, G. Y. Radiation Methods in Nanotechnology. *J. Eng. Phys. Thermophys.* **2011**, *84*, 947–963.
- (37) Coskun, U. C.; Mebrahtu, H.; Huang, P. B.; Huang, J.; Sebba, D.; Biasco, A.; Makarovski, A.; Lazarides, A.; LaBean, T. H.; Finkelstein, G. Single-Electron Transistors Made by Chemical Patterning of Silicon Dioxide Substrates and Selective Deposition of Gold Nanoparticles. *Appl. Phys. Lett.* **2008**, *93*, 123101.
- (38) Domke, J.; Radmacher, M. Measuring the Elastic Properties of Thin Polymer Films with the Atomic Force Microscope. *Langmuir* **1998**, *14*, 3320–3325.
- (39) Lorenz, H.; Despont, M.; Fahrni, N.; LaBianca, N.; Renaud, P.; Vettiger, P. SU-8: A Low-Cost Negative Resist for MEMS. *J. Micromech. Microeng.* **1997**, *7*, 121–124.

- (40) Bojdys, M. J.; Müller, J.-O.; Antonietti, M.; Thomas, A. Ionothermal Synthesis of Crystalline, Condensed, Graphitic Carbon Nitride. *Chemistry* **2008**, *14*, 8177–8182.
- (41) Berthon, L.; Nikitenko, S. I.; Bisel, I.; Berthon, C.; Faucon, M.; Saucerotte, B.; Zorz, N.; Moisy, P. Influence of Gamma Irradiation on Hydrophobic Room-Temperature Ionic Liquids $[\text{BuMeIm}] \text{PF}_6$ and $[\text{BuMeIm}] (\text{CF}_3\text{SO}_2)_2\text{N}$. *Dalton Trans.* **2006**, 2526–2534.
- (42) Reynaud, C.; Sommer, F.; Quet, C.; El Bounia, N.; Duc, T. M. Quantitative Determination of Young's Modulus on a Biphase Polymer System Using Atomic Force Microscopy. *Surf. Interface Anal.* **2000**, *30*, 185–189.
- (43) Laible, R. C. Allyl Polymerizations. *Chem. Rev.* **1958**, *58*, 807–843.
- (44) Noda, A.; Hayamizu, K.; Watanabe, M. Pulsed-Gradient Spin-Echo ^1H and ^{19}F NMR Ionic Diffusion Coefficient, Viscosity, and Ionic Conductivity of Non-Chloroaluminate Room-Temperature Ionic Liquids. *J. Phys. Chem. B* **2001**, *105*, 4603–4610.
- (45) Drouin, D.; Couture, A. R.; Joly, D.; Tastet, X.; Aimez, V.; Gauvin, R. CASINO V2.42: A Fast and Easy-to-Use Modeling Tool for Scanning Electron Microscopy and Microanalysis Users. *Scanning* **2007**, *29*, 92–101.
- (46) Hatzakis, M. New High-Resolution and High-Sensitivity Deep UV, X-Ray, and Electron-Beam Resists. *J. Electrochem. Soc.* **1991**, *138*, 1076.
- (47) Lee, K. Y. Evaluation and Application of a Very High Performance Chemically Amplified Resist for Electron-Beam Lithography. *J. Vac. Sci. Technol., B* **1993**, *11*, 2807.
- (48) Argitis, P. An Advanced Epoxy Novolac Resist for Fast High-Resolution Electron-Beam Lithography. *J. Vac. Sci. Technol., B* **1995**, *13*, 3030.
- (49) Pantenburg, F. J.; Achenbach, S.; Mohr, J. Influence of Developer Temperature and Resist Material on the Structure Quality in Deep X-Ray Lithography. *J. Vac. Sci. Technol., B* **1998**, 3547–3551.
- (50) Ziegler, J. F.; Ziegler, M. D.; Biersack, J. P. SRIM – The Stopping and Range of Ions in Matter. *Nucl. Instruments Methods Phys. Res., Sect. B* **2010**, *268*, 1818–1823.